Biosensors and Bioelectronics 153 (2020) 112038

Contents lists available at ScienceDirect

Biosensors and Bioelectronics

journal homepage: http://www.elsevier.com/locate/bios

Wearable multiplexed biosensor system toward continuous monitoring of metabolites

Murat A. Yokus [a], Tanner Songkakul [a], Vladimir A. Pozdin [b], Alper Bozkurt [a,*], Michael A. Daniele [a,b,*]

[a] Department of Electrical & Computer Engineering, North Carolina State University, 890 Oval Dr., Raleigh, NC, 27695, USA
[b] Joint Department of Biomedical Engineering, North Carolina State University and University of North Carolina at Chapel Hill, 911 Oval Dr., Raleigh, NC, 27695, USA

ARTICLE INFO

Keywords:
Wearable
Multiplex
Potentiostat
Electrochemical sensors
Glucose
Lactate
pH
Sweat sensors

ABSTRACT

Comprehensive metabolic panels are the most reliable and common methods for monitoring general physiology in clinical healthcare. Translation of this clinical practice to personal health and wellness tracking requires reliable, non-invasive, miniaturized, ambulatory, and inexpensive systems for continuous measurement of biochemical analytes. We report the design and characterization of a wearable system with a flexible sensor array for non-invasive and continuous monitoring of human biochemistry. The system includes signal conditioning, processing, and transmission parts for continuous measurement of glucose, lactate, pH, and temperature. The system can operate three discrete electrochemical cells. The system draws 15 mA under continuous operation when powered by a 3.7 V 150 mAh battery. The analog front-end of the electrochemical cells has four potentiostats and three multiplexers for multiplexed and parallel readout from twelve working electrodes. Utilization of redundant working electrodes improves the measurement accuracy of sensors by averaging chronoamperometric responses across the array. The operation of the system is demonstrated *in vitro* by simultaneous measurement of glucose and lactate, pH, and skin temperature. In benchtop measurements, the sensors are shown to have sensitivities of 26.31 μA $mM^{-1}{\cdot}cm^{-2}$ for glucose, 1.49 μA $mM^{-1}{\cdot}cm^{-2}$ for lactate, 54 $mV{\cdot}pH^{-1}$ for pH, and 0.002 $^{\circ}C^{-1}$ for temperature. With the custom wearable system, these values were 0.84 ± 0.03 mV $\mu M^{-1}{\cdot}cm^{-2}$ or glucose, 31.87 ± 9.03 mV $mM^{-1}{\cdot}cm^{-2}$ for lactate, 57.18 ± 1.43 $mV{\cdot}pH^{-1}$ for pH, and 63.4 $\mu V{\cdot}^{\circ}C^{-1}$ for temperature. This miniaturized wearable system enables future evaluation of temporal changes of the sweat biomarkers.

1. Introduction

Wearable health and wellness monitoring systems (wearables) are promising solutions to alleviate the burden of chronic diseases on the healthcare system by eliminating patient's dependence on bulky and expensive lab equipment for point-of-care testing and diagnosis. Chronic diseases, such as cardiovascular disorders, cancer, obesity, and diabetes, are projected to account for almost 75% of all deaths worldwide (WHO, 2003). The development and progression of chronic diseases are dependent on dietary, activity, and metabolic patterns (Willett et al., 2006). Integrating wearables into health and wellness regimens can aid in early diagnosis or management of these diseases. To this end, wearables may improve patient health by providing continuous streams of physiological data to healthcare providers to track biomarkers and quickly identify anomalous or pathological patterns.

Long-term monitoring of metabolic biomarkers is one way of benchmarking general patient wellness. Glucose, oxygen, pH, and lactate are some of the metabolic biomarkers. When monitored continuously, these biomarkers can give insights regarding abrupt or chronic changes of physiology (Phypers and Pierce, 2006). For example, during intense exercise, metabolic production of energy switches from aerobic to anaerobic processes, resulting in lactate accumulation in the blood (Finsterer, 2012). Insufficient supply of glucose or impaired clearance of lactate may jeopardize the viability of many organs and result in emergence of various symptoms that may affect the daily life such as exhaustion, cramps, rapid heart rate, shortness of breath, and rapid decrease in blood pH levels (Rassaei et al., 2014). Therefore, continuous monitoring of these biomarkers may provide longitudinal assessment of the patient's health or real-time actionable information for the healthcare provider.

* Corresponding authors. Department of Electrical & Computer Engineering, North Carolina State University, 890 Oval Dr., Raleigh, NC, 27695, USA.
E-mail addresses: aybozkur@ncsu.edu (A. Bozkurt), mdaniel6@ncsu.edu (M.A. Daniele).

https://doi.org/10.1016/j.bios.2020.112038
Received 24 September 2019; Received in revised form 15 January 2020; Accepted 17 January 2020
Available online 18 January 2020

Although continuous monitoring of metabolic biomarkers can provide new medical insights, clinical characterization of biomarkers traditionally requires expensive equipment, skilled technicians, and long turnaround time (hours or days) with very poor temporal resolution (Tudos et al., 2001); however, with the advent of point-of-care (PoC) devices (*e.g.*, i-STAT®, Abbott), blood metabolite levels can be measured within a few minutes with a single blood draw volume of about 65–95 μL (Martin, 2010) or even less today (<5 μL). PoC devices enable discrete sampling of biomarker levels; however, they cannot measure abrupt or unforeseen fluctuations between discrete measurement times. Current continuous glucose monitoring devices overcome this issue by monitoring the analyte levels from a few weeks (Dexcom G6® and Abbott FreeStyle Libre®) up to three months (Senseonics Eversense®), but they are invasive systems requiring the insertion of a subcutaneous needle or surgical implant (Deiss et al., 2019; Shah et al., 2018).

In the recent decade, a shift toward non-invasive metabolite and electrolyte sensors, based on sweat analysis, has been reported (Bariya et al., 2018; Choi et al., 2018; Heikenfeld et al., 2019) because conventional blood tests for analyzing glucose and lactate levels are invasive and painful. Sweat offers non-invasive and pain-free assessment of biomarkers of human metabolism. Sweat contains biologically relevant ions (*e.g.*, Na^+, Cl^-, K^+, and NH_4^+), small molecules (*e.g.*, ethanol, glucose, lactate, and urea), and small proteins (Bandodkar et al., 2014; Jia et al., 2013; Kim et al., 2015; Sonner et al., 2015). Sweat based sensors have been developed for detection of ethanol (Kim et al., 2016), glucose (Bandodkar et al., 2015), pH and calcium (Emaminejad et al., 2017), and lactate (Jia et al., 2013). For example, lactate in sweat was studied for the characterization of physiological performance, pressure ischemia, cystic fibrosis, and panic disorder (Derbyshire et al., 2012; Tur-Garcia et al., 2017). Despite the ongoing debate regarding the exact correlation between sweat and blood metabolites (Heikenfeld, 2016; Wolfe et al., 1970), there have been recent reports illustrating the correlation between sweat and blood glucose concentrations (Bandodkar et al., 2015; Hong et al., 2018; Lee et al., 2017; Sakharov et al., 2010). Therefore, sweat may present an alternative way of continuous monitoring of overall physiological condition.

Wearable system integration and redundancy are major technical hurdles. First, most reports demonstrate sensors for single analyte detection, which may be insufficient to evaluate the overall health condition. These sensors use a single working electrode, which results in poor reliability due to fundamental sensor failure, sensor delamination from skin surface, or cessation of sweating where the sensor is in contact with the skin. Second, the best performing sensors are demonstrated with benchtop hardware, but they are rarely demonstrated as wearable system-level solutions. To date, there are a few emerging examples of fully-integrated wearables for sweat analysis (Bandodkar et al., 2019; Choi et al., 2019; Gao et al., 2016; Imani et al., 2016; Lee et al., 2017; Lei et al., 2019). These systems monitor levels of sweat metabolites and electrolytes along with additional sensors, such as sweat rate, blood oxygenation, or ECG. The systems use either electrochemical or colorimetric detection techniques for quantification of biomarkers. Selected studies are summarized in Supplementary Table S1. A common feature of these systems, with one exception (Lee et al., 2017), is that they have a single sensing electrode per analyte. This lack of redundancy may yield imprecise or inaccurate results due to sensor-to-sensor variation and operating conditions, which is very common in enzymatic electrochemical sensors used in wearables.

To build on the groundbreaking work by the Heikenfeld, Javey, Kim, and Gao research teams, developing a system with an electrode array for multiple analyte detection and redundancy may mitigate signal reliability issues. First, electrode arrays can be functionalized with various recognition elements so that multiple concurrent tests can be performed. Second, the precision of sensor output can be improved by running simultaneous measurements across multiple electrodes or by including functionalized and non-functionalized electrodes (*i.e.*, positive and negative controls) to subtract the effect of common interferences. Last, multi-biasing can be applied to detect analytes with different redox potentials. However, to provide these benefits, the operation of electrode arrays requires a next-generation of miniaturized and multiplexed electronic hardware.

Accordingly, the use of electrode arrays for the detection of multiple analytes requires a system with signal conditioning modules (biasing, filtering, and amplification) and multiplexing capabilities for each type of sensor. Many single analyte (single electrode) detection systems have been reported, they include custom-designed potentiostats for electrochemical detection of metabolites, heavy metals, drugs, and DNA molecules for applications, such as cellular microphysiometry, wearable sensing, and point-of-care sensing (Supplementary Table S2) (Nemiroski et al., 2014; Rowe et al., 2011; Steinberg et al., 2015). These systems were able to perform electrochemical techniques, such as chronoamperometry, cyclic voltammetry, and square wave voltammetry. Fewer reports have designed systems for multiplexed analyte detection. These designs used either a separate readout unit for each working electrodes (Harrington et al., 1989; Levine et al., 2008; Lima et al., 2014) or multiplexing between an array of working electrodes (Ghoreishizadeh et al., 2014; Yang et al., 2009) (Supplementary Fig. S1). A separate readout unit for each working electrodes offers rapid measurement because of simultaneous measurement functionality but requires a large circuit area. The latter approach uses multiplexing scheme to read from each individual electrode results in an area efficient design, but with a compromise of reduced sampling rate as it scans through an entire array of electrodes. To overcome some of these challenges, a hybrid multiplexing topology was proposed (Hu et al., 2016; Ramfos et al., 2015) (Supplementary Fig. S1d), providing multiplexing and parallelization that results in both reduced circuit area and improved real-time performance. Consequently, a miniaturized and inexpensive hybrid-multiplexing system would enable simultaneous detection of multiple analytes as well as multiplexed reading from redundant electrodes.

Herein, we report an array-based flexible sensor platform integrated with a low-cost multiplexing system for simultaneous detection of glucose, lactate, pH, and temperature. The array of electrodes was fabricated on a flexible thin polymeric film and functionalized via selective electrodeposition. The wearable hardware is a miniaturized and inexpensive stand-alone system, which is fabricated with commercially available discrete components. The custom system consists of analog front-end designs for pH and temperature sensors. It also includes potentiostats along with multiplexers to record from twelve working electrodes designed for glucose and/or lactate sensing. The multiplexing system along with the flexible sensing array presents another step toward an on-body solution for continuous monitoring of metabolic biomarkers.

2. Materials and Methods

2.1. Fabrication of flexible electrode array

A more detailed fabrication procedure is provided in the supplementary text. Briefly, polydimethylsiloxane (10:1 ratio; Sylgard 184, Dow Corning) was spin-coated on a 100 mm glass wafer as a sacrificial layer. The PDMS film was cured at 70 °C for 1.5 h in a vacuum oven. A 50 μm thick polyimide (PI) film was temporarily adhered to the PDMS coated wafer. The wafer was cleaned with acetone and isopropyl alcohol. A Cr/Au thin film (20 nm/300 nm) was deposited on the PI film by DC sputtering. The Cr/Au thin film was patterned by photolithography and wet etching. The conductive traces were encapsulated by spin coating of a positive photoresist (Microposit® S1813). The electrode areas and the pads were exposed by developing the photoresist layer. Additional details are provided in Supplementary Text 1.3 and Supplementary Fig. S2.

2.2. Functionalization of the flexible electrode array

(i) *Electrodeposition of gold nanoparticles.* The surface of planar gold electrodes was cleaned in 50 mM H_2SO_4 solution (product #258105, Sigma-Aldrich) using cyclic voltammetry method from −0.4 to 1 V at a scan rate of 100 mV s^{-1} for 10 cycles. An aqueous solution of 2 mM $HAuCl_4$ (product #254169, Sigma-Aldrich) in 2 M H_2SO_4 (product #258105, Sigma-Aldrich) was prepared. The electrode was dipped in the prepared solution. Gold nanoparticles (AuNPs) were electrodeposited on bare gold electrode surface using chronoamperometric method. The deposition was performed for 15 min at −0.1 V with an external Pt counter electrode and an Ag/AgCl reference electrode (Supplementary Fig. S3a). AuNPs deposited electrodes were used for glucose and lactate sensors.

(ii) *Electrodeposition of Prussian blue.* An aqueous solution of 100 mM KCl (product #746436, Sigma-Aldrich), 2.5 mM $FeCl_3$ (product #97064–656, VWR), and 2.5 mM $K_3Fe(CN)_6$ (product #97062–260, VWR) in 100 mM HCl (product #AAAL13091, VWR) was prepared. The AuNPs deposited gold electrode was dipped into the solution. Prussian blue was electrodeposited by cyclic voltammetry method from 0 to 0.5 V at a scan rate of 20 mV s^{-1} with an external Pt counter electrode and an Ag/AgCl reference electrode (Supplementary Fig. S3c).

(iii) *GOx immobilization.* 5 mg mL^{-1} exfoliated graphite (product #282863, Sigma-Aldrich) solution was prepared in 1X phosphate-buffered saline (PBS) (product #BP2944, Fisher Scientific). The exfoliation process was completed using an ultrasonic bath (product #15337410, Fisher Scientific) for 1.5 h. The exfoliated graphite solution was mixed with GOx (50 mg mL^{-1}, product#G7141, Sigma-Aldrich) and bovine serum albumin (BSA) (10 mg mL^{-1}, product #0332, VWR). GOx/BSA/exfoliated graphite (0.5 μL) was drop-cast on the Prussian blue coated (4 cycles) electrode. The electrodes were kept in ambient temperature for 30 min for drying. Glutaraldehyde solution (0.5 μL of 2 wt %; product #TC0067, VWR) was drop-cast on the electrode and kept in the fridge (4 °C) for drying. Afterwards, 0.8 μL of 0.5 wt % Nafion® (product #70160, Sigma-Aldrich) was drop-cast on the electrode and dried at room temperature.

(iv) *LOx immobilization.* A solution of LOx (50 mg mL^{-1}, product#E2030703P1, Gwent Group) and BSA (10 mg mL^{-1}) was prepared in 1X PBS. LOx and BSA solution (0.4 μL) were drop casted on the Prussian blue coated (20 cycles) planar gold electrode. The electrodes were dried at room temperature for 30 min. Glutaraldehyde solution (0.4 μL of 2 wt %) was drop-cast on the electrode and kept at 4 °C until it was tested. Nafion® (0.8 μL of 0.5 wt %) was drop-cast on the electrode and dried at room temperature. The exfoliated graphite was not used in fabrication of the lactate sensor because its incorporation did not improve the sensitivity of the sensor according to benchtop analysis (Supplementary Fig. S4b).

(v) *Electrodeposition of polyaniline.* An aqueous solution of 0.1 M aniline (product#242284, Sigma-Aldrich) in 1 M HCl was prepared. Polyaniline (PANI) was deposited on the planar gold electrode by cyclic voltammetry method by sweeping the potential from −0.2 to 1 V at a scan rate of 100 mV s^{-1} for 30 cycles with an external Pt counter electrode and an Ag/AgCl reference electrode (Supplementary Fig. S3b).

(vi) *Encapsulation of temperature sensor.* The surface of the temperature sensor was exposed by patterning in the fabrication process. Its surface can be coated with polymeric films to control its thermal properties. In our case, the encapsulation of the temperature sensor was made using liquid bandage spray (Walgreen's).

(vii) *Fabrication of reference electrode.* The reference electrodes of glucose, lactate, pH sensors were fabricated by drop casting an Ag/AgCl ink (product #C2130809D5, Gwent Group) on the planar gold electrodes. The electrodes were subsequently cured at 80 °C for 15 min.

(viii) *Selective functionalization of the electrodes.* Electrodeposition is a technique for selective deposition of various materials on a single platform with minimal cross-contamination. We used electrodeposition of AuNPs and Prussian blue (PB) for fabrication of glucose and lactate sensors. Similarly, polyaniline (PANI) electrodeposition was carried out for fabrication of pH sensors. The selective functionalization of the flexible array started with the electrodeposition PANI on the working electrode of the pH sensor. Then, the sample was cured at 80 °C for 5 min. PANI was chosen due to its surface sensitivity to protonation in different pH solutions. This step was followed with the electrodeposition of AuNPs on the planar gold electrode surface (*i.e.*, working electrodes of glucose and lactate sensors). Afterwards, PB was electrodeposited on the AuNPs electrodes, and the sample was cured at 80 °C for 45 min. PB is selected due to its high catalytic activity towards hydrogen peroxide, which is a byproduct of the reaction between glucose oxidase-glucose or lactate oxidase-lactate. Afterwards, an Ag/AgCl ink was drop casted on the reference electrodes of the pH, glucose, and lactate sensors. The sample was cured at 80 °C for 15 min. Later on, the working electrode surfaces of glucose and lactate sensors were functionalized with GO_x and LO_x enzyme mixtures, respectively. Chemical crosslinking of the enzymes to bovine serum albumin (BSA) was performed with 2% glutaraldehyde solution. Finally, a 0.5% Nafion® film was drop-casted on top of the working electrodes as encapsulation layer. The samples were stored at 4 °C when not in use.

2.3. Characterization of the flexible sensors array

(i) *Characterization of electrodeposited gold nanoparticles.* The characterization of electrodeposited porous gold electrodes was performed by electrochemical impedance spectroscopy (EIS) with a Gamry 600+ benchtop potentiostat. The electrodes were dipped into an aqueous solution of 5 mM $K_3Fe(CN)_6$ in 1X PBS. EIS measurement was performed with an external Pt counter electrode and an Ag/AgCl reference electrode from 1 Hz to 5 MHz ($V_{AC} = 10$ mV and $V_{DC} = 0$ V). Cyclic voltammetry measurements were carried out in an aqueous solution of 10 mM $K_3Fe(CN)_6$ in 1X PBS from −0.3 to 0.9 V with a scan rate of 100 mV s^{-1} with an external Pt counter electrode and an Ag/AgCl electrode. Scanning electron micrographs were obtained with an FEI Verios 460L.

(ii) *Characterization of glucose and lactate sensors.* Chronoamperometric characterization of glucose and lactate sensors were performed with a Gamry 600+ benchtop potentiostat at −0.1 V in 1X PBS solution. A conditioning step was performed at −0.1 V. A steady state current was obtained after 10 min. Measurements of glucose or lactate were made at 5 min intervals to ensure a homogenous solution. Chronoamperometric measurement were made at −0.1 V for 100 s.

(iii) *Characterization of* pH *and temperature sensors.* Open circuit potential measurements (OCP) in buffer solutions (pH = 4.0–8.0, Fisher Scientific) were performed with a benchtop Gamry 600+ potentiostat. The PANI deposited electrodes were dipped into the buffer solutions and OCP readings were carried out for 5 min. The characterization of the temperature sensor was performed on a hot plate. Resistance measurements were performed to calibrate the temperature sensor as the hot plate temperature was changed from 22 °C to 45 °C at a rate of 1 °C·min^{-1}. The temperature sensor was brought in contact with the surface of the hot plate. A K-type surface thermocouple with adhesive backing was adhered next to the sensor to measure the surface temperature of the hot plate. The temperature sensor was connected to source measure unit (B2902a, Keysight) for resistance measurement. A custom-

designed LabVIEW script was used to measure the surface thermocouple temperature and the resistance change of the temperature sensor.

(iv) *Intraelectrode and interelectrode crosstalk study.* Intraelectrode crosstalk test was performed in aqueous solution of 5 mM $K_3Fe(CN)_6$ and 1 M KCl in 1X PBS. Four carbon-working electrodes (product# RRPE1001C, PINE Research) were electrically connected to $WE_{1\text{-}1}$, $WE_{1\text{-}2}$, $WE_{1\text{-}3}$, and $WE_{1\text{-}4}$ of the first channel ($WE_{x\text{-}y}$, for *x*: 1,2,3 and *y*: 1,2,3,4, where *x* and *y* indicate the channel number and the working electrode number, respectively). The counter and reference electrode inputs of the potentiostat were connected to an external Pt counter electrode and an Ag/AgCl reference electrode. The carbon electrodes were conditioned in the same aqueous solution at −0.1 V. A steady state current was obtained after 30 min. A PANI coated carbon electrode and an Ag/AgCl reference electrode (PINE Research) were used as pH sensors. Afterwards, the intraelectrode crosstalk test was started. The reference and working electrode of the pH sensor were disconnected after 10 min. Similarly, $WE_{1\text{-}4}$, $WE_{1\text{-}3}$, and $WE_{1\text{-}2}$ were disconnected at 15, 20, and 25 min, respectively. The overall test was completed in 30 min.

For interelectrode crosstalk, new carbon electrodes were electrically connected to the $WE_{1\text{-}1}$, $WE_{2\text{-}1}$, and $WE_{3\text{-}1}$ of the first, second, and the third channels of the multiplexing system. The electrodes were then dipped into a similar aqueous solution and preconditioning step was completed at the same conditions as the intraelectrode crosstalk study. The interelectrode crosstalk study was performed by disconnecting the reference and working electrode of the pH sensor after 10 min. Similarly, $WE_{3\text{-}1}$ and $WE_{2\text{-}1}$ were disconnected at 15 and 20 min, respectively. The overall test was completed in 25 min. The temperature sensor was not involved in the crosstalk test since its surface is encapsulated and thus insulated from crosstalk.

(v) *Off-body measurement of sampled sweat.* The off-body evaluation of the custom multiplexing system was performed in compliance with the protocol that was approved by the Institutional Review Board at University of North Carolina, Chapel Hill (#18–0984). Three healthy subjects (1 female and 2 males), aged 18–35 exercised on a cycle ergometer (Life Sciences ® 95Ri recumbent exercise bike) and sweat samples were collected after a period of constant workload. The power output was monitored through the cycle ergometer. For the constant workload exercise, the subjects exercised at 50 W for 5 min. The workload was increased to 150 W and the exercise was maintained at this workload for 20 min. Then, it was followed by recovery and cool-down at 50 W for 5 min. The cycling was kept at 60 rpm for all exercise levels. Sweat was collected in the 20 min intense exercise period from the forehead of the subjects. Off-body measurement of the collected sweat samples were performed by the custom-designed multiplexing system. The system was also tested with a stabilized artificial sweat solution (product#1700–0020, Pickering Laboratories) as a reference. The artificial sweat solution includes 19 different amino acids, 4 metabolites (uric acid, urea, lactic acid, and ammonia), and 8 different minerals. For our measurements, 200 μM glucose was added to the artificial sweat solution since it did not contain glucose. The concentration of glucose and lactate in the collected and artificial sweat was measured using colorimetric glucose (Amplex™ Red Glucose Assay Kit, product#A22189, ThermoFisher Scientific) and lactate (Amplite™ L-Lactate Assay Kit, product#13815, AAT Bioquest) assay kits. Black non-binding (product# 07000634, Fisher Scientific) and white medium binding (product# 07000097, Fisher Scientific) 96 well plates were used for glucose and lactate assays, respectively.

3. Results and discussion

3.1. Design of flexible sensor array and custom multiplexing system

The design of the flexible sensor array (length: 28 mm, width: 22 mm) is shown in Fig. 1. The sensor was fabricated on a polyimide film to form a flexible sensor. The sensor is comprised of a layered structure (Fig. 1a): polyimide (bottom), metallization (intermediate), and encapsulation (top) layers. The metallization layer allows the various sensors along with their corresponding electrical contact pads to be easily inserted into a surface mount connector on the custom-built printed circuit board (PCB) (Fig. 1b). The flexible sensor array consists of a total of twelve (12) working electrodes along with three reference and counter electrodes for glucose, lactate, and background current (Supplementary Fig. S6a). The array also has a serpentine resistive temperature sensor and a pair of electrodes for pH sensing (Fig. 1c). Each channel has a three-electrode electrochemical cell configuration with an array of four working electrodes ($WE_{1\text{-}1}$ to $WE_{1\text{-}4}$, $WE_{2\text{-}1}$ to $WE_{2\text{-}4}$, and $WE_{3\text{-}1}$ to $WE_{3\text{-}4}$), a reference and a counter electrode. The working electrodes in each individual channel have been either functionalized for amperometric detection of glucose and lactate or left blank for background current detection. The four working electrodes in each channel are connected to a potentiostat through a multiplexer in the custom designed system (Fig. 1d and Supplementary Fig. S6a).

A four-layer PCB was designed to interface with the flexible sensor (Fig. 1b). The system consists of six different units: system-on-chip (a microcontroller with wireless transceiver), three multiplexing units for glucose and lactate sensors, four potentiostats, a pH-sensing unit, a temperature-sensing unit, and a power management unit (Fig. 1d). The system-on-chip (SoC) is a Bluegiga BLE113 Bluetooth® Smart Module and provides the processing and communication capability. The SoC coordinates proper switching between working electrodes, data processing, and wirelessly transmits to a data aggregator, such as a smartphone or tablet via Bluetooth Low Energy (BLE). The multiplexers are connected to three potentiostats (LMP91000, Texas Instruments). To measure different analyte concentrations, the three potentiostats are configured as three-lead electrochemical cells, one potentiostat for each of the analyte channels. Each analyte channel contains four working electrodes, one reference and one counter electrode (Supplementary Fig. S6a). The fourth potentiostat is used for generating 1 V virtual ground. The four working electrodes of each potentiostat are connected to an 8-channel single-pole, single-throw (SPST) switch (MAX14662, Maxim Integrated) to multiplex between the four working electrodes. In total, twelve I^2C controlled single pull single throw (SPST) switches can be toggled to connect each of the four electrodes on each analyte channel to the potentiostat individually. Twelve additional SPST switches connect each of the electrodes to a virtual ground, which matches the virtual ground internal to the potentiostat. This creates a software-controlled make-before-break single-pull double-throw (SPDT) switch for each working electrode wherein each working electrode is connected to the virtual ground when not in use (Supplementary Fig. S1d and Fig. S6b). This is necessary because multiplexing with break-before-make SPDT switches or simply using SPST switches between the working electrodes and the potentiostat creates intermittent biasing, which disrupts the electrochemical processes of the cell (Ramfos et al., 2013). The LMP91000 also contains a transimpedance amplifier with adjustable gain, which allows for measurement of very high and very low analyte concentrations without saturation or inadequate precision (Supplementary Table S3 and Supplementary Figs. S7a–b). The pH-sensing unit (LMP91200, Texas Instruments) performs the pH measurement between a reference electrode and pH indicator electrode. The temperature-sensing unit measures temperature via a voltage divider (10 kΩ). The potentiostat outputs, pH, and temperature measurements are all read by the microcontroller via 16-bit analog-to-digital converters (ADS1115, Texas Instruments). The power management circuit of the system starts with a 3.7 V, 150 mAh lithium-polymer battery to

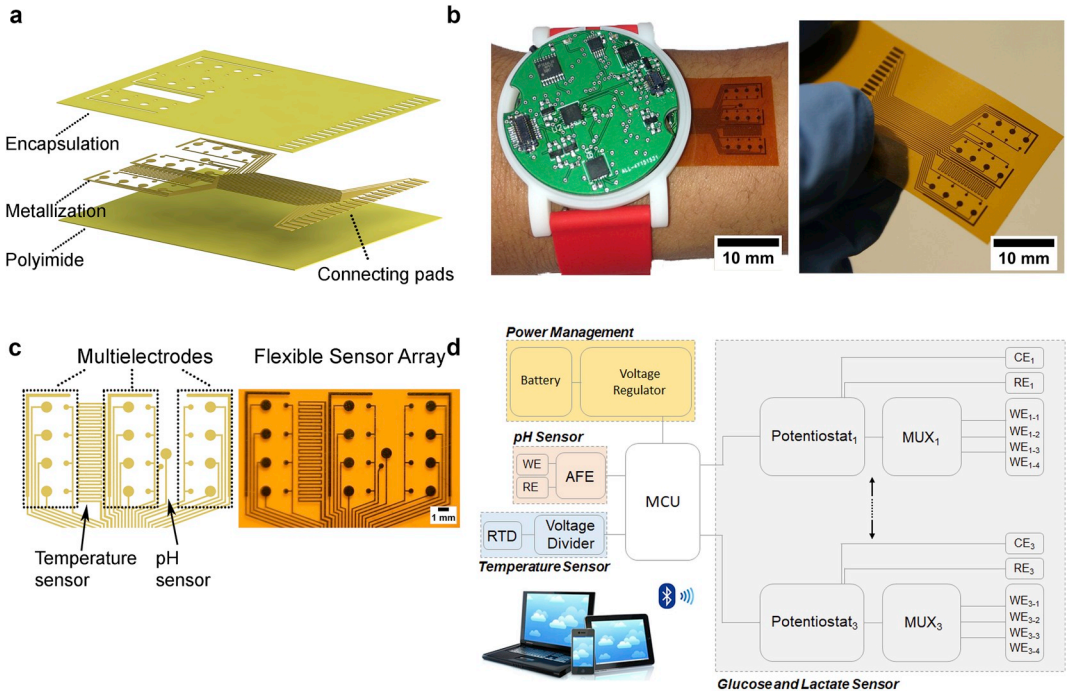

Fig. 1. Images and system block diagram of the custom multiplexing system along with a flexible sensor array. **(a)** Exploded view of the flexible sensor array showing the polyimide (bottom), metallization (intermediate), and encapsulation (top) layers. **(b)** *Left:* Picture of wrist-worn, wearable multiplexing system in a 3D printed watch enclosure for demonstration purposes only. *Right:* Picture of the flexible sensor array. **(c)** *Left:* CAD design of the flexible sensor array. *Right:* Fabricated flexible sensor array. **(d)** System block diagram of the custom multiplexing sensor system.

power the device. This battery can be charged by a 5 V external power supply (USB) through a battery management and a fuel gauge integrated circuit (MCP73831, Microchip). To increase power efficiency, switching regulators are utilized for the voltage rails of the device. The battery voltage is regulated to 3.3 V by a step down converter (TPS62162, Texas Instruments) in order to power the microcontroller and peripherals. The 3.3 V rail is boosted up to 5 V by a boost converter (TPS61222, Texas Instruments). The 5 V rail serves as a reference for the potentiostat and increases range of voltage sweeps. A pushbutton controller (MAX16054, Maxim Integrated) allows the user to power the device on and off.

Overall, the system can perform concurrent cyclic voltammetry (CV) sweeps on all 12 channels between −1.2 V and 1.2 V at sweep rates between 10 mV s^{-1} and 1000 mV s^{-1} with a 0.1 V step size, while simultaneously measuring pH and temperature. Alternatively, the system can carry out concurrent chronoamperometric measurement of all 12 channels at a sampling rate of 10 Hz, again while measuring pH and temperature. The system is powered by a 3.7 V 150 mAh battery and consumes around 15 mA when actively measuring analyte concentrations and transmitting data, giving a battery life of 9.9 h for continuous measurement and wireless data transmission. The system consumes 60 μA when in idle mode, allowing for a drastic reduction in average power consumption for applications in which intermittent sampling is appropriate. For example, reducing sampling rate by sampling for 30 s and then entering idle mode for 10 min decreases the average current consumption to 0.25 mA s^{-1} and extends battery lifetime to 600 h. The final system has a diameter of 40 mm and a thickness of 9 mm. The custom multiplexing potentiostat system costs $92 each at prototype quantities, with significant cost reduction possible at higher production quantities. The summary of specifications of the custom designed potentiostat, the specifications of the components used in the custom system is provided in Supplementary Tables S3–S5 and Supplementary Figs. S8 and S9.

3.2. In-vitro characterization of glucose, lactate, pH, and temperature sensors

The concentration of glucose and lactate in sweat depends on various factors such as sampling site, sampling techniques, participant's age, diet, degree of acclimation, gender, race, and activity levels (Stefaniak and Harvey, 2006). Sweat concentrations are different from blood concentrations and have been reported to be 5.6 μM to 2.2 mM for glucose and 3.7 mM–50 mM for lactate (Boysen et al., 1984; Harvey et al., 2010; Sonner et al., 2015). Median concentrations for glucose and lactate are reported to be 170 μM and 14 mM, respectively (Harvey et al., 2010). A wide working range, fast response, and interference-free operation is required for continuous monitoring of sweat metabolites.

The fabrication of glucose and lactate sensors started with electrodeposition of gold nanoparticles on the planar gold electrodes (Supplementary Text 1.4, Supplementary Fig. S3a and Fig. S10). 15 min gold deposition time was used because the deposition time was sufficient to cover the surface of the bare gold electrodes. After 15 min of the porous gold deposition, the electrochemically active surface area increased by 1.38 times (Supplementary Table S6), which decreased the DC electrode impedance by two orders of magnitude (Supplementary Fig. S11a) and resulted in 1.36 times increased current (Supplementary Figs. S11b–c).

We first characterized the sensors using a benchtop potentiostat. The chronoamperometric response of glucose and lactate sensors are shown in Fig. 2a and Fig. 2c respectively. The response of glucose and lactate sensors were separately recorded using a benchtop potentiostat at a constant potential of −0.1 V vs. an Ag/AgCl reference electrode for 100 s in 1X PBS solution. The operation potential was selected based on electro-oxidation of glucose and lactate by the fabricated flexible sensor during cyclic voltammetry tests. When the sensor is exposed to glucose or lactate in the solution, GOx or LOx enzymes catalyzes the oxidation of metabolites and generates gluconic acid and pyruvate, respectively (Wang, 2008). Both reactions generate hydrogen peroxide (H_2O_2) that is reduced by the Prussian blue mediator, leading to a change in the cathodic current (Karyakin, 2017). The cathodic detection of H_2O_2 at

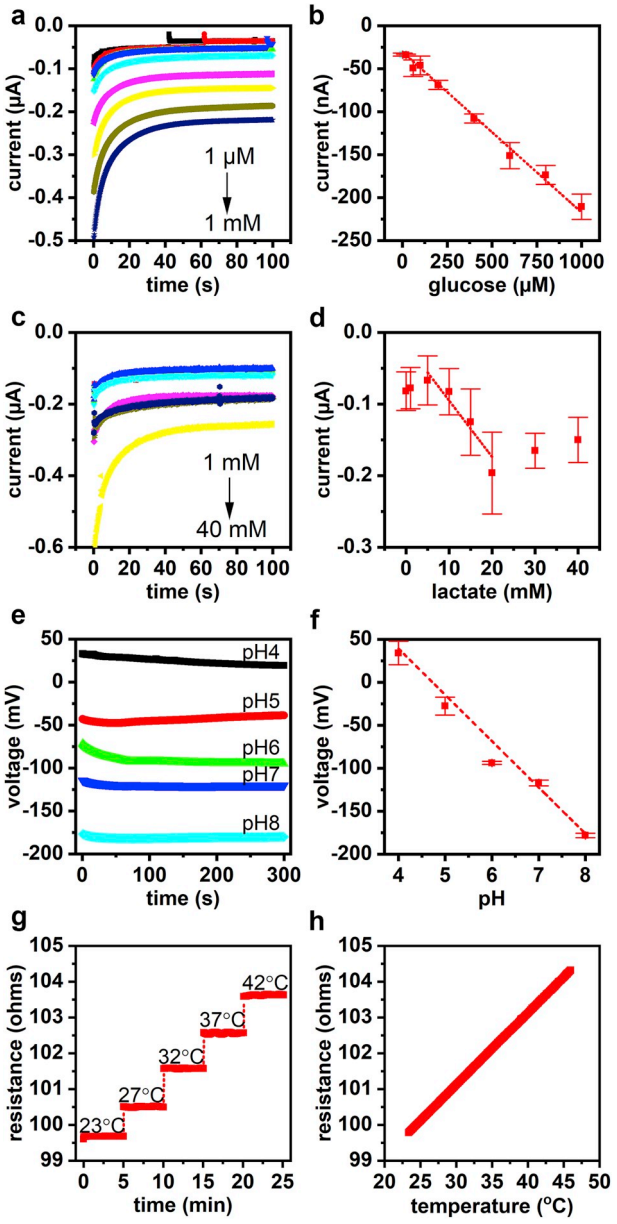

Fig. 2. Characterization of the fabricated flexible sensor array with a benchtop potentiostat. Working electrode area: 0.0071 cm^2. **(a–d)** Chronoamperometric responses of the glucose **(a,b)** and lactate **(c,d)** sensors with increasing glucose (0–1000 μM) and lactate (0–40 mM) concentration in 1X PBS solution (n = 3). Bias: −0.1 V, pH 7.4, at 21 °C. **(e–f)** Open circuit potential response of the pH sensor for increasing pH levels (n = 3). **(g–h)** Resistance response of the temperature sensor to temperature changes (22–45 °C). The plots on the second column shows the corresponding calibration plots of the glucose, lactate, pH, and temperature sensors in the physiological relevant ranges.

low potentials eliminates interferences from other oxidizable metabolites in sweat (*e.g.*, uric acid and ascorbic acid) (Mickelsen and Keys, 1943; O'Halloran et al., 2001; Stefaniak and Harvey, 2006). The chronoamperometric response of the glucose and lactate sensors to increasing glucose and lactate concentrations are shown in Fig. 2a–b and Fig. 2c–d. The linear range of the sensors were 60 μM–1000 μM and 5 mM–20 mM for glucose and lactate sensors, respectively. While the linear range of the lactate sensors cover both blood and interstitial fluid levels, the linear region of the lactate sensor could be further extended to cover sweat levels by decreasing the diffusion coefficient of the lactate through the encapsulation layer (*i.e.*, selection of proper encapsulation layer material with a different substrate permeability), selecting a different electron-transfer system, or increasing the thickness of the encapsulation layer (Payne et al., 2019; Rathee et al., 2016; Han et al., 2007; Lyons, 2006; Stikoniene et al., 2010). Such improvements may come at a cost of reduced signal magnitude.

The sensitivity of the glucose and lactate sensors were 26.31 ± 0.63 μA $mM^{-1}{\cdot}cm^{-2}$ (or 0.186 ± 0.004 μA mM^{-1}) and 1.49 ± 0.20 μA $mM^{-1}{\cdot}cm^{-2}$ (or 0.011 ± 0.002 μA mM^{-1}), respectively. The specifications of the sensors fabricated in this study fall within specifications of the previously reported glucose and lactate sensors that are characterized with a benchtop potentiostat (Supplementary Tables S7 and S8). The differences in fabrication methods (*e.g.*, drop casting, layer-by-layer deposition, or electrodeposition), materials (*e.g.*, electrode, nanoparticles, and encapsulating film), test conditions (*e.g.*, applied potential, pH of test solution, stirring effect) results in sensors with varying specifications. The storage stability of the sensors was tested by keeping the fabricated sensors in a sealed Petri dish at 4 °C in a fridge. The sensitivity of the glucose and lactate sensors decreased to 8.96 ± 0.65 μA $mM^{-1}{\cdot}cm^{-2}$ (or 0.064 ± 0.005 μA mM^{-1}) and 0.23 ± 0.08 μA $mM^{-1}{\cdot}cm^{-2}$ (or 0.002 ± 0.001 μA mM^{-1}) after 10 days storage, respectively (Supplementary Fig. S5).

Sweat pH varies between 4.0 and 8.0 during an intense exercise (Patterson et al., 2000; Robergs et al., 2004). In our flexible sensor array, we electrodeposited electrically conductive polyaniline polymer as a pH sensor (Supplementary Fig. S3b), whose protonation strongly depends on the oxidation state of the polymer and the pH of the aqueous solution (Song and Choi, 2013). The pH sensor was calibrated with standard buffer solutions (Fig. 2e). The open circuit potential of the sensor vs. printed Ag/AgCl reference electrode decreased in high pH buffer solutions due to deprotonation of the polyaniline. The sensitivity of the pH sensor was 54 ± 3.61 $mV{\cdot}pH^{-1}$ (Fig. 2f). The sensitivity of the PANI pH sensor falls between the sensitivity range of other polymer or oxide-based pH sensors (40–61 $mV{\cdot}pH^{-1}$) (Chung et al., 2014; Nyein et al., 2016; Salvo et al., 2017). The sensors showed good repeatability in successive measurements of pH in buffer solutions (Supplementary Fig. S3d).

Human skin temperature is dependent on body core temperature, ambient conditions, and exercise intensity, and it varies between roughly 25–40 °C (Abe et al., 1980; Saltin et al., 1972). A skin conformable temperature sensor should be sensitive to the variations in skin temperature. The serpentine-shaped temperature sensor on the flexible sensor array (Fig. 1c) is made of a thin chromium/gold layer, whose resistance varies with temperature (Fig. 2g and h). As the temperature increases, the thermal vibrations of the atoms in the solid lattice increases (*i.e.*, phonons). The likelihood of electrons and phonons collision increases, resulting in a resistance increase. The temperature coefficient of resistance (α) of the sensor was calculated as 0.002 $°C^{-1}$. The temperature coefficient values were similar to other thin-film-based (*e.g.*, platinum or gold) temperature sensors (Chen et al., 2015; Lacy, 2009).

3.3. System validation of the custom multiplexing system

The custom system was validated using commercial electrodes as controls. First, cyclic voltammetry measurements of the ferricyanide/ferrocyanide redox reaction were performed to demonstrate the operation of the custom hardware. A carbon working electrode, an Ag/AgCl reference electrode, and a Pt counter electrode were used for all tests. The electrodes were submerged an aqueous solution of 5 mM $K_3Fe(CN)_6$ and 1 M KCl (Fig. 3e and f). Similar cyclic voltammetry tests were also repeated with a benchtop potentiostat. The ferricyanide/ferrocyanide redox potentials and peak amplitudes obtained with the custom system and the benchtop potentiostat were identical (Fig. 3a,e). In cyclic voltammetry experiments, the resolution of the applied bias in our system was set as a percentage of the reference voltage in the potentiostat. The resolution of the applied bias in the custom designed potentiostat is 0.1 V, which is less than the resolution of the commercial benchtop

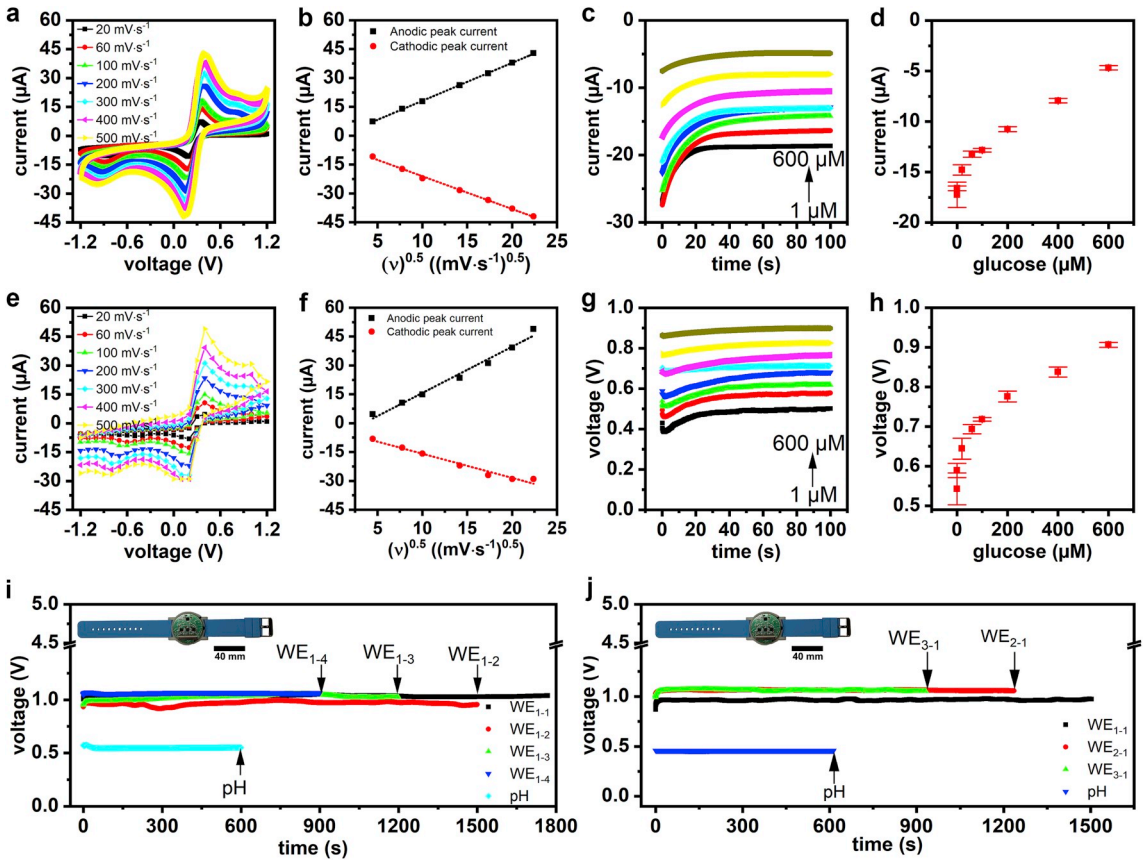

Fig. 3. System validation of the custom multiplexing system. **(a, b)** Benchtop potentiostat cyclic voltammetry and peak current vs. square root of scan rate graphs in 5 mM $K_3Fe(CN)_6$ and 1 M KCl in 1X PBS. R^2 is 0.99 for both anodic and cathodic peaks. **(c, d)** Chronoamperometry measurements with a benchtop potentiostat in an aqueous solution of GO_x (10 mg mL^{-1}) and $K_3Fe(CN)_6$ (10 mg mL^{-1}) in 1X PBS solution (n = 3). Bias: −0.1 V, pH 7.4. **(e, f)** Custom system cyclic voltammetry and peak current vs. square root of scan rate graphs in an aqueous solution of 5 mM $K_3Fe(CN)_6$ and 1 M KCl in 1X PBS. R^2 is 0.98 and 0.97 for anodic and cathodic peaks, respectively. **(g, h)** Chronoamperometry measurements with the custom system in an aqueous solution of GO_x (10 mg mL^{-1}) and $K_3Fe(CN)_6$ (10 mg mL^{-1}) in 1X PBS (n = 3). Bias: −0.1 V, pH 7.4. **(i)** Intraelectrode crosstalk study within the same channel. "*$WE_{1\text{-}1}$, $WE_{1\text{-}2}$, $WE_{1\text{-}3}$, and $WE_{1\text{-}4}$*": First, second, third, and fourth working electrodes of the first channel, respectively. **(j)** Interelectrode crosstalk study among different channels. "*$WE_{1\text{-}1}$, $WE_{2\text{-}1}$, and $WE_{3\text{-}1}$*": The first working electrode of the first, second, and third channels. Each arrow on the graphs indicates the time when the given electrode is electrically disconnected.

potentiostat (0.2 mV) (Supplementary Table S3). The resolution of the applied bias could be further increased by decreasing the reference voltage of the potentiostat. The peak current of oxidation and reduction was proportional to the square root of the scan rate, indicating that the surface reaction on the electrode is reversible and diffusion-controlled (Fig. 3b,f). Similarly, we verified the chronoamperometric response of our custom system by performing standard enzymatic glucose and lactate assays. The enzymatic oxidation of glucose (1 μM–600 μM) and lactate (1 mM–40 mM) were measured in corresponding enzyme and mediator solutions (*i.e.*, $GO_x + K_3Fe(CN)_6$ in 1X PBS or $LO_x + K_3Fe(CN)_6$ in 1X PBS) (Fig. 3g and h and Supplementary Figs. S12c and d and Figs. S12g and h). The same experiments were also repeated with the benchtop potentiostat (Fig. 3c and d and Supplementary Figs. S12a and b and Figs. S12e and f). Our custom designed system was able to differentiate the addition of glucose or lactate into the cell similarly to the benchtop potentiostat. It is important to note that magnitude of the cathodic current decreased as we increased the concentration of glucose or lactate in the test solution, which was different from the response when the enzyme was functionalized on the electrode surface (Fig. 2a and b). This different trend may be attributed to the electron transport differences between enzyme and the electrode surface when they are either immobilized on an electrode surface or dispersed in an aqueous solution. Since glucose does not dissociate into ions in water, increasing the glucose concentration in the test solution and conformational changes of the protein make it even more difficult to transfer the electrons from redox site of the enzyme to the electrode surface.

It is crucial to have a crosstalk-free operation of glucose, lactate, pH, and temperature sensors fabricated as a part of the flexible sensor array. The intraelectrode crosstalk is defined as the interference between the four working electrodes for a given channel. Similarly, the interelectrode crosstalk is defined as the interference between the working electrodes of the three separate channels. Thus, we performed intra-electrode and interelectrode crosstalk tests in an aqueous solution to investigate potential interference from surrounding electrodes. For the intraelectrode crosstalk test, four working electrodes (*i.e.*, commercial carbon electrodes) with shared common and reference electrodes of one potentiostat and pH electrodes were submerged into the test solution (explained in detail in Materials and Methods section). In case of the interelectrode crosstalk test, only the first working electrode of each channel, separate counter and reference electrodes, and the pH electrodes were submerged into the test solution. Only the first electrode of each channel is used because one working electrode is electrically connected to a potentiostat per channel for a given time. After the signal acquisition was started, the electrodes were disconnected sequentially to observe if there would be any shift in baseline current. Any shift in the baseline current would indicate a possible crosstalk. It was demonstrated that disconnecting each working electrode sequentially in the intraelectrode test did not cause any intermittent noise in the chronoamperometric readings of the surrounding electrodes since the working electrodes were connected to the virtual ground when they were not in use (Fig. 3i and Supplementary Figs. S6a–b). In the typical operation, such as intraelectrode switching, the SPDT multiplexer

connects only one working electrode to the potentiostat with a working electrode bias of 1 V and all the others to the virtual ground of 1 V. Similarly, there was no interelectrode crosstalk observed (Fig. 3j).

With the sensors characterized with the benchtop potentiostat in the Section 3.2, we proceeded to measure our sensors with the custom multiplexing system. The chronoamperometric responses of the glucose and lactate sensors were tested separately in the range of 0–1000 μM and 0–40 mM in 1X PBS, respectively (Fig. 4a and c). The cathodic current increased with addition of glucose or lactic acid into the test solution. In the wearable system, the output of sensors were plotted in volts, which can be further converted to current using the Supplementary Table S3. The glucose sensor showed a linear response up to 1000 μM, while the lactate sensor showed a linear response up to 15 mM. The small variation of the linear region of the lactate sensor may be attributed to process

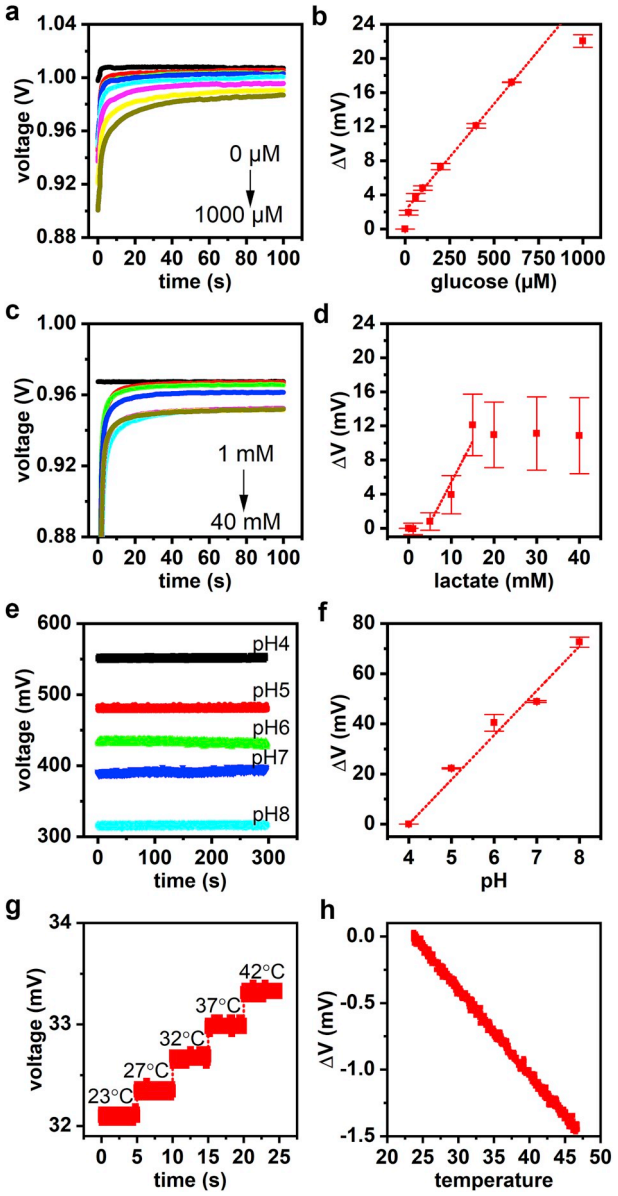

Fig. 4. Characterization of the fabricated flexible sensor array with the custom multiplexing system. **(a–d)** Chronoamperometric responses of the glucose **(a,b)** and lactate **(c,d)** sensors for increasing glucose (0–1000 μM) and lactate (0–40 mM) concentrations in 1X PBS (n = 3). Bias: 0.1 V, pH 7.4. **(c)** Open circuit potential response of the pH sensor for increasing pH levels (4–8). **(d)** Voltage response of the temperature sensor to variations in temperature (23–42 °C). **(e–g)** The corresponding calibration plots of the glucose, lactate, and pH sensors, respectively.

variability of the drop-casting method. The sensitivity of glucose and lactate sensors with the custom PCB was 0.84 ± 0.03 mV $\mu M^{-1} \cdot cm^{-2}$ and 31.87 ± 9.03 mV $mM^{-1} \cdot cm^{-2}$, respectively. The amperometric signal measured with the custom PCB system was noisier than the signal acquired by the benchtop potentiostat due to an advanced filtering in the benchtop potentiostat. Therefore, a moving average with a window size of 11 was applied to smooth the chronoamperometric data. To minimize the effect of sample-to-sample variation during the sensor fabrication caused by the electrodeposition, drop casting, and the contribution of the other electrical interferences, the calibration graphs of the glucose and lactate sensor with the custom system were plotted as voltage difference ($\Delta V = V_{0\ mM} - V_{final\ concentration}$) vs. concentration in Fig. 4b and d. Similarly, Fig. 4e and f shows the voltage output of the pH sensor in the buffer solutions from pH 4 to 8. The pH response of the sensors decreased as the test solution became more basic, similarly to the benchtop system measurements ($\Delta V = V_{final\ pH} - V_{pH4}$). The sensitivity of the sensor with the custom system was calculated as 57.18 ± 1.43 $mV \cdot pH^{-1}$. Fig. 4g and h shows the response of the temperature sensor when the temperature was varied from 23 to 42 °C. The sensitivity of the sensor with the custom system was calculated to be 63.4 $\mu V \cdot °C^{-1}$ ($\Delta V = V_{23°C} - V_{final\ temperature}$).

3.4. Simultaneous measurement of glucose, lactate, pH, and temperature

The multiplexing system with the flexible sensor array was evaluated by sequential addition of glucose and lactic acid into the test solution (sampling frequency = 10 Hz). The full data was provided in Supplementary Fig. S13 and Fig. S14 for successive additions of 200, 400, and 600 μM of glucose and 5, 10, and 15 mM of lactic acid into the test solution with 5 min intervals. The unfiltered response of sensors to 400 μM glucose and 10 mM lactic acid additions is shown in Fig. 5a and b, respectively.

Addition of glucose into the test solution resulted in a drop in the cathodic current in all working electrodes that were functionalized for glucose sensing (WE_{1-1} to WE_{1-4}). The output of the four glucose sensors were slightly different due to the variations in their fabrication processes. It was reported that use of multiple (redundant) electrodes for sensing of a specific analyte improved the accuracy, consistency, and reliability of measurement in amperometric measurements (Schmidtke et al., 1996; Sharifi et al., 2016; Ward et al., 2003). These improvements were achieved by either combining the mean or median of multiple WEs outputs or applying intelligent algorithms with time-varying weight factors. In our case, the effect of sensor-to-sensor variation on the determination of the concentration of glucose in the solution was minimized by averaging the responses of the four glucose sensors. The concentration of the glucose in the solution was calculated using the voltage output of the system and the sensitivity of the glucose sensor. The baseline current did not change for the blank electrodes (WE_{2-1} to WE_{2-4}), lactate sensors, and pH sensors after the glucose addition. During testing, the addition of the test solution created noise because of the disruption of the electrode-electrolyte interface (grey regions in Fig. 5a and b). The responses of all sensors to 10 mM lactic acid solution are shown in Fig. 5b. The lactate sensors (WE_{3-1} to WE_{3-4}) responded to the lactic acid addition with a decrease in cathodic current. The concentration of the lactic acid in the solution was calculated using the average output of the lactate sensors. The calculated lactate concentration showed an increase in lactic acid levels. Furthermore, the addition the lactic acid into the solution lowered the overall pH of the solution, which was detected with a sharp peak in the output of the pH sensor. This caused the calculated pH values to be close to zero upon the initial addition of lactic acid, but a steady-state level was reached (pH 4.8) as the lactic acid diffused through the solution. This sudden change may be due to the voltage change across the reference electrode with the lactic acid addition, which could be minimized by encapsulating the reference electrode with NaCl loaded polymeric membranes (Guinovart et al., 2014). Similar pH sensor trend was observed for 5 and 15 mM lactic acid

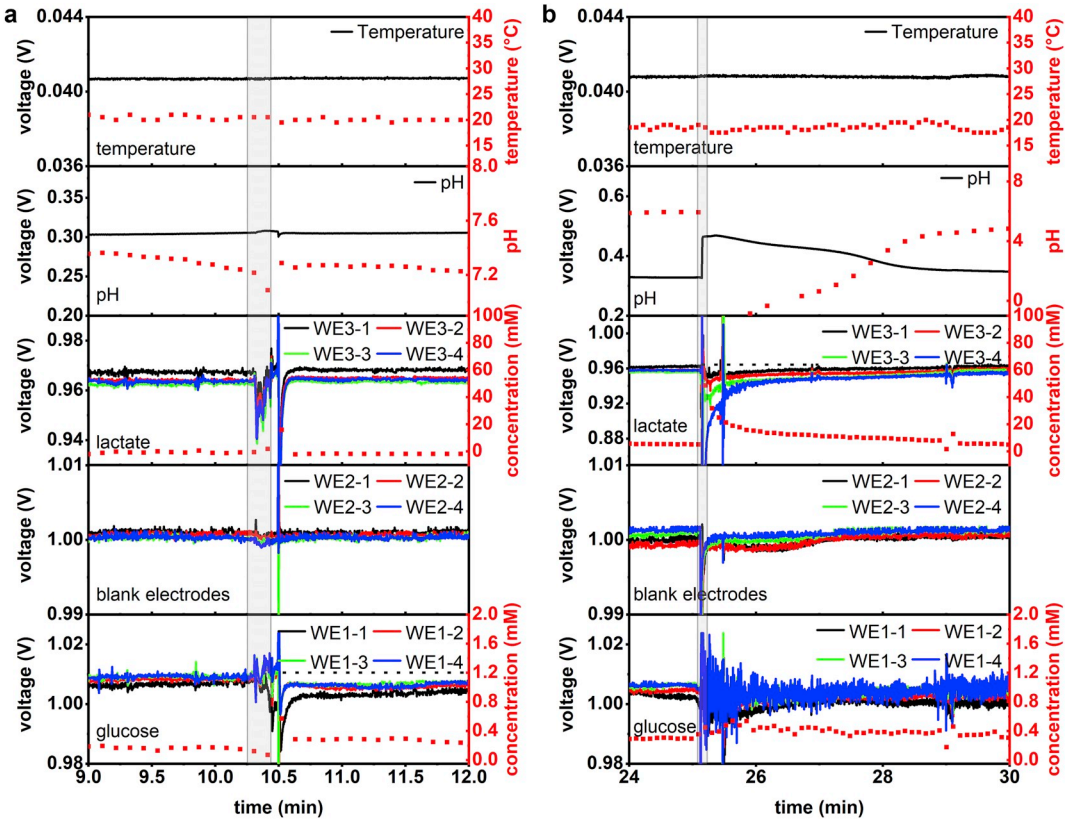

Fig. 5. Multiplexed reading of glucose, lactate, pH, and temperature with a custom-designed multiplexed system in 1X PBS solution. The plots are replotted from the highlighted regions of the Supplementary Fig. S13. (a) Multiplexed measurement of glucose, lactate, pH, and temperature after addition of glucose into the test solution (final concentration of glucose in the test solution: 400 μM). **(b)** Multiplexed measurement of glucose, lactate, pH, and temperature after addition of lactic acid into the test solution (final concentration of lactic acid in the test solution: 10 mM). Conditions of the chronoamperometric measurements (bias: −0.1 V, pH: 7.4, working electrode area: 0.03 cm^2). The grey highlighted region in **(a)** and **(b)** shows the noise generated due to pipetting the analyte solution into the test solution. WE_{1-1} to WE_{1-4}: glucose sensors, WE_{2-1} to WE_{2-4}: blank electrodes, WE_{3-1} to WE_{3-4}: lactate sensors (WE_{x-y}, for x: 1,2,3 and y: 1,2,3,4, where x and y indicate the channel number and the working electrode number, respectively).

additions as well (Supplementary Fig. S13 and Fig. S14). The output of the glucose sensors and blank working electrodes slightly changed by the lactic acid addition. The change in the response of the glucose sensor may be attributed to variation in electrochemical activity of the Prussian blue mediator and glucose oxidase in acidic solutions. The lactic acid addition created significant noise in WE_{1-4} (glucose sensor). However, the effect of the lactic acid addition on the calculation of glucose concentration in the solution was minimized by averaging the responses of four glucose sensors (WE_{1-1} to WE_{1-4}). The output of the temperature sensor did not change throughout the testing. The grey highlighted regions in Fig. 5 shows generated noise due to motion artifacts. The motion artifacts were introduced due to the variations of the speed and the volume of the pipetting as well as the sensor movement throughout the duration of the measurement. In wearable sweat sensing applications, the fluid management for the wearable sensor is not going to include pipetting volumes of analytes; therefore, this type of noise generation may not be experienced.

Off-body analysis of collected sweat samples was performed with the multiplexed sensing system. Approximately 1.2 mL of sweat was collected from Subject 1 and 2. The amount of sweat collected from the last subject was less than 200 μL; therefore, it was not included in the testing. The concentration of glucose and lactate in the collected sweat samples were quantified with commercial fluorometric and colorimetric assays (Supplementary Table S9). The as-collected concentration of glucose was 24.25 μM and 40.17 μM for Subject 1 and 2, respectively. The as-collected concentration of lactate was 40.36 mM and 39.35 mM for Subject 1 and 2, respectively. The as-collected sweat sample (150 μL) was drop-casted on the flexible sensor and its multiplexed analysis was performed with the custom system. The results are shown for the both subjects in Supplementary Fig. S15 and Fig. S16. To test the response of the custom system in real sweat samples, glucose and lactate were supplemented into the as-collected sweat samples; an additional amount of 1 mM glucose solution and 1 M lactic acid solution were sequentially added to the sample volume. For both subjects, response of the custom system was as expected. The addition of glucose and lactic acid to the as-collected sweat sample resulted in a decrease in the sensor's output (*i.e.*, increased enzymatic current generation). The output of the pH sensor increased (*i.e.*, became more acidic) and the output of the temperature sensor remained unchanged. Similar tests were repeated with a commercial, artificial sweat solution and showed comparable trends in the sensor outputs (Supplementary Fig. S17).

It is important to note that the sensors in our study were calibrated in 1X PBS solution in Fig. 4. While the relative response of the sensors to different analyte concentrations was comparable, the absolute values of the sensor output varied across the different media, *i.e.* human sweat versus 1X PBS. For example, the absolute current generation of lactate sensor in 1X PBS was higher than absolute current generation of the artificial sweat with added lactic acid (Supplementary Fig. S17b). This suggests that the calibration curves or reference tables for the sensors must be developed in comparable, complex media compositions and conductivities. If calibration curves of the enzymatic sensors are generated in simplified conditions, operation in real sweat may lead to innacruate calculation of the true concentrations of metabolites. To minimize this error, future calibration of such sensors should be performed in artificial sweat solution that has similar composition and conductivity as real sweat, or the system can be used to make relative

response measurements after setting a baseline value in the operational media, *e.g.* sweat, saliva, or interstitial fluid.

4. Conclusion

In this study, we have demonstrated a custom designed multiplexing system with a flexible sensor array for a multiplexed detection of glucose, lactate, pH, and temperature. The flexible sensor array is disposable and can be easily mounted on the custom-designed board for multiplexed, wireless, simultaneous, and continuous readout from all sensors. Utilization of the custom multiplexing system enables fast and simultaneous readout from multiple working electrodes. The custom multiplexing system consumes 15 mA during active measurement and data transmission, costs $92 per unit, and has a wearable form factor ($40 \times 40 \times 9$ mm). The system demonstrates comparable performance to benchtop hardware for conventional cyclic voltammetry and chronoamperometry. In vitro tests demonstrated that the system can quantify and discriminate between two metabolic biomarkers present in sweat—glucose and lactate. These measurements are made in parallel with the characterization of pH and temperature in typical physiological ranges. Utilization of the redundant electrodes along with the custom multiplexing system enables accurate calculation of the analyte levels in the test solution. Future work will focus on further optimization of the system at different pH and temperatures for compensating any potential enzymatic activity loss of the glucose and lactate sensors. This wearable system is a promising demonstration of the necessary measurement tools for non-invasive, wireless, and continuous electrochemical measurement of biomarkers in sweat.

Declaration of competing interest

The authors declare that they have no known competing financial interests or personal relationships that could have appeared to influence the work reported in this paper.

CRediT authorship contribution statement

Murat A. Yokus: Investigation, Methodology, Formal analysis, Visualization, Writing - original draft. **Tanner Songkakul:** Investigation, Software, Writing - review & editing. **Vladimir A. Pozdin:** Investigation, Writing - review & editing. **Alper Bozkurt:** Conceptualization, Writing - review & editing, Supervision, Funding acquisition. **Michael A. Daniele:** Conceptualization, Methodology, Writing - original draft, Supervision, Project administration, Funding acquisition.

Acknowledgements

This work was done in collaboration with the National Science Foundation (EEC1160483) through a NSF Nanosystems Engineering Research Center (NERC) for Advanced Self-Powered Systems of Integrated Sensors and Technologies (ASSIST). This work was performed in part at the NCSU Nanofabrication Facility (NNF), a member of the North Carolina Research Triangle Nanotechnology Network (RTNN), which is supported by the National Science Foundation (Grant ECCS-1542015) as part of the National Nanotechnology Coordinated Infrastructure (NNCI).

Appendix A. Supplementary data

Supplementary data to this article can be found online at https://doi.org/10.1016/j.bios.2020.112038.

References

Abe, T., Mayuzumi, J., Kikuchi, N., Arai, S., 1980. Seasonal-variations in skin temperature, skin ph, evaporative water-loss and skin surface lipid values on human-skin. Chem. Pharm. Bull. 28 (2), 387–392.

Bandodkar, A.J., Gutruf, P., Choi, J., Lee, K., Sekine, Y., Reeder, J.T., Jeang, W.J., Aranyosi, A.J., Lee, S.P., Model, J.B., Ghaffari, R., Su, C.-J., Leshock, J.P., Ray, T., Verrillo, A., Thomas, K., Krishnamurthi, V., Han, S., Kim, J., Krishnan, S., Hang, T., Rogers, J.A., 2019. Battery-free, skin-interfaced microfluidic/electronic systems for simultaneous electrochemical, colorimetric, and volumetric analysis of sweat. Sci. Adv. 5 (1).

Bandodkar, A.J., Jia, W.Z., Yardimci, C., Wang, X., Ramirez, J., Wang, J., 2015. Tattoo-based noninvasive glucose monitoring: a proof-of-concept study. Anal. Chem. 87 (1), 394–398.

Bandodkar, A.J., Molinnus, D., Mirza, O., Guinovart, T., Windmiller, J.R., Valdés-Ramírez, G., Andrade, F.J., Schöning, M.J., Wang, J., 2014. Epidermal tattoo potentiometric sodium sensors with wireless signal transduction for continuous non-invasive sweat monitoring. Biosens. Bioelectron. 54, 603–609.

Bariya, M., Nyein, H.Y.Y., Javey, A., 2018. Wearable sweat sensors. Nat. Electron 1 (3), 160–171.

Boysen, T.C., Yanagawa, S., Sato, F., Sato, K., 1984. A modified anaerobic method of sweat collection. J. Appl. Physiol. 56 (5), 1302–1307.

Chen, Y., Lu, B.W., Chen, Y.H., Feng, X., 2015. Breathable and stretchable temperature sensors inspired by skin. Sci. Rep. 5.

Choi, J., Bandodkar, A.J., Reeder, J.T., Ray, T.R., Turnquist, A., Kim, S.B., Nyberg, N., Hourlier-Fargette, A., Model, J.B., Aranyosi, A.J., Xu, S., Ghaffari, R., Rogers, J.A., 2019. Soft, skin-integrated multifunctional microfluidic systems for accurate colorimetric analysis of sweat biomarkers and temperature. ACS Sens. 4 (2), 379–388.

Choi, J., Ghaffari, R., Baker, L.B., Rogers, J.A., 2018. Skin-interfaced systems for sweat collection and analytics. Sci. Adv. 4 (2).

Chung, H.J., Sulkin, M.S., Kim, J.S., Goudeseune, C., Chao, H.Y., Song, J.W., Yang, S.Y., Hsu, Y.Y., Ghaffari, R., Efimov, I.R., Rogers, J.A., 2014. Stretchable, multiplexed pH sensors with demonstrations on rabbit and human hearts undergoing ischemia. Adv. Healthc. Mater. 3 (1), 59–68.

Deiss, D., Szadkowska, A., Gordon, D., Mallipedhi, A., Schutz-Fuhrmann, I., Aguilera, E., Ringsell, C., De Block, C., Irace, C., 2019. Clinical practice recommendations on the routine use of Eversense, the first long-term implantable continuous glucose monitoring system. Diabetes Technol. Ther. 21 (5), 254–264.

Derbyshire, P.J., Barr, H., Davis, F., Higson, S.P.J., 2012. Lactate in human sweat: a critical review of research to the present day. J. Physiol. Sci. 62 (6), 429–440.

Emaminejad, S., Gao, W., Wu, E., Davies, Z.A., Nyein, H.Y.Y., Challa, S., Ryan, S.P., Fahad, H.M., Chen, K., Shahpar, Z., Talebi, S., Milla, C., Javey, A., Davis, R.W., 2017. Autonomous sweat extraction and analysis applied to cystic fibrosis and glucose monitoring using a fully integrated wearable platform. Proc. Natl. Acad. Sci. 114 (18), 4625–4630.

Finsterer, J., 2012. Biomarkers of peripheral muscle fatigue during exercise. Bmc Musculoskel. Dis. 13.

Gao, W., Emaminejad, S., Nyein, H.Y.Y., Challa, S., Chen, K., Peck, A., Fahad, H.M., Ota, H., Shiraki, H., Kiriya, D., Lien, D.-H., Brooks, G.A., Davis, R.W., Javey, A., 2016. Fully integrated wearable sensor arrays for multiplexed in situ perspiration analysis. Nature 529 (7587), 509–514.

Ghoreishizadeh, S.S., Baj-Rossi, C., Cavallini, A., Carrara, S., De Micheli, G., 2014. An integrated control and readout circuit for implantable multi-target electrochemical biosensing. IEEE Trans. Biomed. Circuits Syst. 8 (6), 891–898.

Guinovart, T., Crespo, G.A., Rius, F.X., Andrade, F.J., 2014. A reference electrode based on polyvinyl butyral (PVB) polymer for decentralized chemical measurements. Anal. Chim. Acta 821, 72–80.

Han, J.H., Taylor, J.D., Kim, D.S., Kim, Y.S., Kim, Y.T., Cha, G.S., Nam, H., 2007. Glucose biosensor with a hydrophilic polyurethane (HPU) blended with polyvinyl alcohol/vinyl butyral copolymer (PVAB) outer membrane. Sens. Actuators, B 123 (1), 384–390.

Harrington, M.S., Anderson, L.B., Robbins, J.A., Karweik, D.H., 1989. Multiple electrode potentiostat. Rev. Sci. Instrum. 60 (10), 3323–3328.

Harvey, C.J., LeBouf, R.F., Stefaniak, A.B., 2010. Formulation and stability of a novel artificial human sweat under conditions of storage and use. Toxicol. In Vitro 24 (6), 1790–1796.

Heikenfeld, J., 2016. Non-invasive analyte access and sensing through eccrine sweat: challenges and outlook circa 2016. Electroanalysis 28 (6), 1242–1249.

Heikenfeld, J., Jajack, A., Feldman, B., Granger, S.W., Gaitonde, S., Begtrup, G., Katchman, B.A., 2019. Accessing analytes in biofluids for peripheral biochemical monitoring. Nat. Biotechnol. 37 (4), 407–419.

Hong, Y.J., Lee, H., Kim, J., Lee, M., Choi, H.J., Hyeon, T., Kim, D.H., 2018. Multifunctional wearable system that integrates sweat-based sensing and vital-sign monitoring to estimate pre-/post-exercise glucose levels. Adv. Funct. Mater. 28 (47).

Hu, Y.X., Sharma, S., Weatherwax, J., Cass, A., Georgiou, P., 2016. A portable multi-channel potentiostat for real-time amperometric measurement of multi-electrode sensor arrays. Ieee Int. Symp. Circ. S 1306–1309.

Imani, S., Bandodkar, A.J., Mohan, A.M.V., Kumar, R., Yu, S.F., Wang, J., Mercier, P.P., 2016. A wearable chemical-electrophysiological hybrid biosensing system for real-time health and fitness monitoring. Nat. Commun. 7.

Jia, W., Bandodkar, A.J., Valdés-Ramírez, G., Windmiller, J.R., Yang, Z., Ramírez, J., Chan, G., Wang, J., 2013. Electrochemical tattoo biosensors for real-time noninvasive lactate monitoring in human perspiration. Anal. Chem. 85 (14), 6553–6560.

Karyakin, A.A., 2017. Advances of Prussian blue and its analogues in (bio)sensors. Curr. Opin. Electrochem. 5 (1), 92–98.

Kim, J., de Araujo, W.R., Samek, I.A., Bandodkar, A.J., Jia, W.Z., Brunetti, B., Paixao, T. R.L.C., Wang, J., 2015. Wearable temporary tattoo sensor for real-time trace metal monitoring in human sweat. Electrochem. Commun. 51, 41–45.

Kim, J., Jeerapan, I., Imani, S., Cho, T.N., Bandodkar, A., Cinti, S., Mercier, P.P., Wang, J., 2016. Noninvasive alcohol monitoring using a wearable tattoo-based iontophoretic-biosensing system. ACS Sens. 1 (8), 1011–1019.
Lacy, F., 2009. Using nanometer platinum films as temperature sensors (constraints from experimental, mathematical, and finite-element analysis). IEEE Sens. J. 9 (9), 1111–1117.
Lee, H., Song, C., Hong, Y.S., Kim, M.S., Cho, H.R., Kang, T., Shin, K., Choi, S.H., Hyeon, T., Kim, D.H., 2017. Wearable/disposable sweat-based glucose monitoring device with multistage transdermal drug delivery module. Sci. Adv. 3 (3).
Lei, Y., Zhao, W., Zhang, Y., Jiang, Q., He, J.-H., Baeumner, A.J., Wolfbeis, O.S., Wang, Z. L., Salama, K.N., Alshareef, H.N., 2019. A MXene-based wearable biosensor system for high-performance in vitro perspiration analysis. Small 15 (19), 1901190.
Levine, P.M., Gong, P., Levicky, R., Shepard, K.L., 2008. Active CMOS sensor array for electrochemical biomolecular detection. IEEE J. Solid State Circuits 43 (8), 1859–1871.
Lima, E.A., Snider, R.M., Reiserer, R.S., McKenzie, J.R., Kimmel, D.W., Eklund, S.E., Wikswo, J.P., Cliffel, D.E., 2014. Multichamber multipotentiostat system for cellular microphysiometry. Sens. Actuators B Chem. 204, 536–543.
Lyons, M.E.G., 2006. Modelling the transport and kinetics of electroenzymes at the electrode/solution interface. Sensors-Basel 6 (12), 1765–1790.
Martin, C.L., 2010. I-STAT – combining chemistry and haematology in PoCT. Clin. Biochem. Rev. 31 (3), 81–84.
Mickelsen, O., Keys, A., 1943. The composition of sweat, with special reference to the vitamins. J. Biol. Chem. 149 (2), 479–490.
Nemiroski, A., Christodouleas, D.C., Hennek, J.W., Kumar, A.A., Maxwell, E.J., Fernandez-Abedul, M.T., Whitesides, G.M., 2014. Universal mobile electrochemical detector designed for use in resource-limited applications. Proc. Natl. Acad. Sci. 111 (33), 11984–11989.
Nyein, H.Y.Y., Gao, W., Shahpar, Z., Emaminejad, S., Challa, S., Chen, K., Fahad, H.M., Tai, L.C., Ota, H., Davis, R.W., Javey, A., 2016. A wearable electrochemical platform for noninvasive simultaneous monitoring of Ca2+ and pH. ACS Nano 10 (7), 7216–7224.
O'Halloran, M.P., Pravda, M., Guilbault, G.G., 2001. Prussian Blue bulk modified screen-printed electrodes for H2O2 detection and for biosensors. Talanta 55 (3), 605–611.
Patterson, M.J., Galloway, S.D.R., Nimmo, M.A., 2000. Variations in regional sweat composition in normal human males. Exp. Physiol. 85 (6), 869–875.
Payne, M.E., Zamarayeva, A., Pister, V.I., Yamamoto, N.A.D., Arias, A.C., 2019. Printed, flexible lactate sensors: design considerations before performing on-body measurements. Sci. Rep. Uk 9.
Phypers, B., Pierce, J.T., 2006. Lactate physiology in health and disease. Cont. Educ. Anaesth. Crit. Care Pain 6 (3), 128–132.
Ramfos, I., Blionas, S., Birbas, A., 2015. Architecture of a modular, multichannel readout system for dense electrochemical biosensor microarrays. Meas. Sci. Technol. 26 (1).
Ramfos, I., Vassiliadis, N., Blionas, S., Efstathiou, K., Fragoso, A., O'Sullivan, C.K., Birbas, A., 2013. A compact hybrid-multiplexed potentiostat for real-time electrochemical biosensing applications. Biosens. Bioelectron. 47, 482–489.
Rassaei, L., Olthuis, W., Tsujimura, S., Sudholter, E.J.R., van den Berg, A., 2014. Lactate biosensors: current status and outlook. Anal. Bioanal. Chem. 406 (1), 123–137.
Rathee, K., Dhull, V., Dhull, R., Singh, S., 2016. Biosensors based on electrochemical lactate detection: a comprehensive review. Biochem. Biophys. Rep. 5, 35–54.
Robergs, R.A., Ghiasvand, F., Parker, D., 2004. Biochemistry of exercise-induced metabolic acidosis. Am. J. Physiol. Reg. I 287 (3), R502–R516.
Rowe, A.A., Bonham, A.J., White, R.J., Zimmer, M.P., Yadgar, R.J., Hobza, T.M., Honea, J.W., Ben-Yaacov, I., Plaxco, K.W., 2011. Cheap stat: an open-source, "do-it-yourself" potentiostat for analytical and educational applications. PLoS One 6 (9), e23783.
Sakharov, D.A., Shkurnikov, M.U., Vagin, M.Y., Yashina, E.I., Karyakin, A.A., Tonevitsky, A.G., 2010. Relationship between lactate concentrations in active muscle sweat and whole blood. Bull. Exp. Biol. Med. 150 (1), 83–85.
Saltin, B., Stolwijk, J.A., Bergh, U., Gagge, A.P., 1972. Body temperatures and sweating during exhaustive exercise. J. Appl. Physiol. 32 (5), 635-&.
Salvo, P., Calisi, N., Melai, B., Cortigiani, B., Mannini, M., Caneschi, A., Lorenzetti, G., Paoletti, C., Lomonaco, T., Paolicchi, A., Scataglini, I., Dini, V., Romanelli, M., Fuoco, R., Di Francesco, F., 2017. Temperature and pH sensors based on graphenic materials. Biosens. Bioelectron. 91, 870–877.
Schmidtke, D.W., Pishko, M.V., Quinn, C.P., Heller, A., 1996. Statistics for critical clinical decision making based on readings of pairs of implanted sensors. Anal. Chem. 68 (17), 2845–2849.
Shah, V.N., Laffel, L.M., Wadwa, R.P., Garg, S.K., 2018. Performance of a factory-calibrated real-time continuous glucose monitoring system utilizing an automated sensor applicator. Diabetes Technol. Ther. 20 (6), 428–433.
Sharifi, A., Varsavsky, A., Ulloa, J., Horsburgh, J.C., McAuley, S.A., Krishnamurthy, B., Jenkins, A.J., Colman, P.G., Ward, G.M., MacIsaac, R.J., Shah, R., O'Neal, D.N., 2016. Redundancy in glucose sensing:enhanced accuracy and reliability of an electrochemical redundant sensor for continuous glucose monitoring. J. Diab. Sci. Technol. 10 (3), 669–678.
Song, E., Choi, J.W., 2013. Conducting polyaniline nanowire and its applications in chemiresistive sensing. Nanomater. Basel 3 (3), 498–523.
Sonner, Z., Wilder, E., Heikenfeld, J., Kasting, G., Beyette, F., Swaile, D., Sherman, F., Joyce, J., Hagen, J., Kelley-Loughnane, N., Naik, R., 2015. The microfluidics of the eccrine sweat gland, including biomarker partitioning, transport, and biosensing implications. Biomicrofluidics 9 (3), 031301.
Stefaniak, A.B., Harvey, C.J., 2006. Dissolution of materials in artificial skin surface film liquids. Toxicol. In Vitro 20 (8), 1265–1283.
Steinberg, M.D., Kassal, P., Kerekovic, I., Steinberg, I.M., 2015. A wireless potentiostat for mobile chemical sensing and biosensing. Talanta 143, 178–183.
Stikoniene, O., Ivanauskas, F., Laurinavicius, V., 2010. The influence of external factors on the operational stability of the biosensor response. Talanta 81 (4–5), 1245–1249.
Tudos, A.J., Besselink, G.A.J., Schasfoort, R.B.M., 2001. Trends in miniaturized total analysis systems for point-of-care testing in clinical chemistry. Lab Chip 1 (2), 83–95.
Tur-Garcia, E.L., Davis, F., Collyer, S.D., Holmes, J.L., Barr, H., Higson, S.P.J., 2017. Novel flexible enzyme laminate-based sensor for analysis of lactate in sweat. Sens. Actuators B Chem. 242, 502–510.
Wang, J., 2008. Electrochemical glucose biosensors. Chem. Rev. 108 (2), 814–825.
Ward, W.K., Casey, H.M., Quinn, M.J., Federiuk, I.F., Wood, M.D., 2003. A fully implantable subcutaneous glucose sensor array: enhanced accuracy from multiple sensing units and a median-based algorithm. Diabetes Technol. Ther. 5 (6), 943–952.
WHO, 2003. Diet, Nutrition and the Prevention of Chronic Diseases. World Technical Report Series, Geneva.
Willett, W.C., Koplan, J.P., Nugent, R., Dusenbury, C., Puska, P., Gaziano, T.A., 2006. Prevention of chronic disease by means of diet and lifestyle changes. In: Disease Control Priorities in Developing Countries, second ed., pp. 833–850.
Wolfe, S., Cage, G., Epstein, M., Tice, L., Miller, H., Gordon Jr., R.S., 1970. Metabolic studies of isolated human eccrine sweat glands. J. Clin. Investig. 49 (10), 1880–1884.
Yang, C., Huang, Y., Hassler, B.L., Worden, R.M., Mason, A.J., 2009. Amperometric electrochemical microsystem for a miniaturized protein biosensor array. IEEE Trans. Biomed. Circuits Syst. 3 (3), 160–168.